Atmos. Chem. Phys. Discuss., 15, 23089–23130, 2015
www.atmos-chem-phys-discuss.net/15/23089/2015/
doi:10.5194/acpd-15-23089-2015

Atmospheric Chemistry and Physics Discussions

Sources of nitrogen deposition in Federal Class I areas in the US

H.-M. Lee[1], F. Paulot[2], D. K. Henze[3], K. Travis[4], D. J. Jacob[4], L. H. Pardo[5], and B. A. Schichtel[6]

[1]Department of Civil, Environmental, and Architectural Engineering, University of Colorado, Boulder, CO, USA
[2]Geophysical Fluid Dynamics Laboratory and Princeton University, Princeton, NJ, USA
[3]Department of Mechanical Engineering, University of Colorado, Boulder, CO, USA
[4]School of Engineering and Applied Sciences, Harvard University, Cambridge, MA, USA
[5]USDA Forest Service, Northern Research Station, University of Vermont Aiken Center, Burlington, VT, USA
[6]Cooperative Institute for Research in the Atmosphere, Colorado State University, Fort Collins, CO, USA

Received: 15 July 2015 – Accepted: 27 July 2015 – Published: 27 August 2015

Correspondence to: H.-M. Lee (hyungmin.lee@colorado.edu)

Published by Copernicus Publications on behalf of the European Geosciences Union.

Abstract

It is desired to control excessive reactive nitrogen (Nr) deposition due to its detrimental impact on ecosystems. Using a 3-dimensional atmospheric chemical transport model, GEOS-Chem, Nr deposition in the contiguous US and eight selected Class I areas (Voyageurs (VY), Smoky Mountain (SM), Shenandoah (SD), Big Bend (BB), Rocky Mountain (RM), Grand Teton (GT), Joshua Tree (JT), and Sequoia (SQ)) is investigated. First, modeled Nr deposition is compared with National Trends Network (NTN) and Clean Air Status and Trends Network (CASTNET) measurements. The seasonality of measured species is generally well represented by the model ($R^2 > 0.6$), except in JT. While modeled Nr is generally within the range of seasonal observations, large overestimates are present in sites such as SM and SD in the spring and summer (up to 0.6 kg N ha^{-1} month^{-1}), likely owing to model high-biases in surface HNO_3. The contribution of non-measured species (mostly dry deposition of NH_3) to total modeled Nr deposition ranges from 1 to 55 %. The spatial distribution of the origin of Nr deposited in each Class I area and the contributions of individual emission sectors are estimated using the GEOS-Chem adjoint model. We find the largest role of long-range transport for VY, where 50% (90%) of annual Nr deposition originates within 670 (1670) km of the park. In contrast, the Nr emission footprint is most localized for SQ, where 50 % (90 %) of the deposition originates from within 130 (370) km. Emissions from California contribute to the Nr deposition in remote areas in the western US (RM, GT). Mobile NO_x and livestock NH_3 are found to be the major sources of Nr deposition in all sites except BB, where contributions of NO_x from lightning and soils to natural levels of Nr deposition are significant (~ 40 %). The efficiency in terms of Nr deposition per kg emissions of NH_3-N, NO_x-N, and SO_2-S are also estimated. Unique seasonal features are found in JT (opposing efficiency distributions for winter and summer), RM (large fluctuations in the range of effective regions), and SD (upwind NH_3 emissions hindering Nr deposition). We also evaluate the contributions of emissions to the total area of Class I regions in critical load exceedance, and to the total magnitude of exceedance. We find

ACPD
15, 23089–23130, 2015

that while it is effective to control emissions in the western US to reduce the area of regions in CL exceedance, it can be more effective to control emissions in the eastern US to reduce the magnitude of Nr deposition above the CL. Finally, uncertainty in the nitrogen deposition caused by uncertainty in the NH_3 emission inventory is explored by comparing results based on two different NH_3 inventories; noticeable differences in the emission inventories and thus sensitivities of up to factor of four found in individual locations.

1 Introduction

Excessive deposition of reactive nitrogen (Nr) is of interest due to its cascading impact on the environment (Vitousek et al., 1997). The primary impacts of Nr deposition appear in terrestrial and aquatic ecosystems as imbalanced nutrition (Galloway et al., 2003), decreased biological diversity (Sala et al., 2000; Stevens et al., 2004; Clark et al., 2013), eutrophication (Fenn et al., 2003; Duce et al., 2008), and acidification (Galloway et al., 2003; Sullivan et al., 2005). Each of these primary impacts lead to subsequent consequences such as disturbances in ecosystems (Galloway et al., 2003) and changes in greenhouse gas emissions and uptakes (Gruber and Galloway, 2008; Reay et al., 2008).

The potential impact of Nr deposition on ecosystems can be evaluated using critical loads (CLs), a quantitative estimate of an exposure to one or more pollutants below which no significant harmful effects occur over the long term (Nilsson, 1988). The magnitude of the CL varies across different types of receptors, e.g., alpine lakes, lichens in forests, alpine vegetation, etc. It can be estimated using various methods (Pardo et al., 2011), which include empirical studies (Bobbink et al., 2010), steady-state mass balance approach (UBA, 2004), and dynamic modeling (Vries et al., 2010). Pardo et al. (2011) synthesized current research related to Nr deposition and comprehensively assessed empirical CLs for major ecoregions across the US.

ACPD
15, 23089–23130, 2015

National Parks (Organic Act of 1916, 16 USC 1–4) and wilderness areas (Wilderness Act of 1964, 16 USC 1131–1136) in the US are required to be protected to conserve natural and historic objects and the wildlife therein. Of these, Federal Class I areas are defined as those where visibility is important (Clean Air Act Amendments of 1977, 40 CFR 81). In the US, current Nr deposition exceeds CLs in many Class I areas. Fenn et al. (2010) estimated that one-third of the land area of California vegetation types is in excess of the CL for Nr deposition. Bowman et al. (2012) empirically determined CLs for vegetation and soils in Rocky Mountain National Park and found ongoing vegetation change due to excessive Nr deposition. Benedict et al. (2013a) found substantial exceedance of CLs for Nr deposition in Grand Teton National Park. Ellis et al. (2013) estimated that exceedances will become more pervasive in the coming decades.

It is desired to reduce the number of regions in CL exceedance and the amount of excessive Nr deposited above CLs. To reach this goal, it is necessary to understand the sources contributing to Nr deposition, which include both natural and anthropogenic emissions of NO_x and NH_3. Chemical transport models (CTM) can be used to study sources of Nr deposition. Zhang et al. (2012) used a 3-D CTM, GEOS-Chem, to investigate the distribution, sources, and processes of Nr deposition in the US. By toggling emissions on and off in consecutive model simulations, they found that Nr deposition was dominated by contributions from domestic NO_x and NH_3 emissions, followed by natural and foreign sources. While this approach provided estimates of the role of the net emissions from these sectors throughout the US, refined estimates of source contributions from specific locations can be calculated using the adjoint of a CTM, which is a computationally efficient tool for such sensitivity analysis (Henze et al., 2009). For example, Paulot et al. (2013) used the adjoint method to identify the sources and processes that control Nr deposition in biodiversity hotspots worldwide and two US national parks (Cuyahoga and Rocky Mountain) and found that anthropogenic sources dominate deposition at all continental sites and are mainly located with 1000 km of the hotspots themselves.

ACPD
15, 23089–23130, 2015

The purpose of this study is to evaluate the origin of Nr that specifically impacts Federal Class I areas throughout the US, identifying the source locations, species and sectors that contribute to both total deposition and deposition above CLs. The results can thus be used to identify how regionally specific emissions mitigation efforts will impact ecosystems in these protected areas. To accomplish this goal, we evaluate source contributions to the collection of all Class I areas as well as eight specific regions: Voyageurs national park (VY), Smoky Mountain national park (SM), Shenandoah national park (SD), Big Bend national park (BB), Rocky Mountain national park (RM), Grand Teton national park (GT), Joshua Tree wilderness (JT), and Sequoia national park (SQ). Following Ellis et al. (2013), we use the lowest estimate of CL for these areas from Pardo et al. (2011) which are based on CLs for lichens in most regions because lichen is among the most sensitive bio-indicators of N in terrestrial ecosystems. These specific areas are selected as they have low CLs (VY, SM, SD, BB, JT: 3 kg N ha^{-1} yr^{-1}, RM, GT, SQ: 2.5 kg N ha^{-1} yr^{-1}) and are thus most likely impacted by Nr deposition. We also choose this set of areas to highlight different spatial distributions of sources and mechanisms governing Nr deposition in regions of the country that are spatially disparate, are subject to a range of nitrogen emission profiles, encompass several types of ecosystems (see Fig. 1), and are subject to Nr deposition at levels close to or above CLs.

The organization of this manuscript is as follows. Modeled seasonality of Nr deposition is compared with measurement data in Sect. 3.1. Sensitivity analysis using the adjoint model is presented in Sect. 3.2. In Sect. 3.3, we examine the impacts of uncertainties in our model's NH_3 emissions in the source attribution results. The paper concludes with summary and discussions in Sect. 4.

ACPD
15, 23089–23130, 2015

2 Methods

2.1 Measurement data

The National Trends Network (NTN) (http://nadp.sws.uiuc.edu) of the National Atmospheric Deposition Program (NADP, 2015) provides weekly records of precipitation amount and chemical properties (i.e., ion concentration, acidity, and conductance) at as many as 250 sites across the US. Rainfall is recorded to the nearest 0.01 inch with a weighing-bucket rain gauge at each site. Chemical properties are analyzed at the Central Analytical Laboratory (NADP, 2015). We use monthly aggregate wet deposition of NH_4^+ and NO_3^- for select sites. However, no data are available for SQ in JJA. For GT, we use Yellowstone and Pinedale, WY, measurements and show the average of them because there is no wet deposition measurement made in 2010 in GT. For RM, there are three collocated monitoring sites, and we use the average of them.

The Clean Air Status and Trends Network (CASTNET, http://epa.gov/castnet) measures ambient concentration of nitrogen, sulfur, and ozone weekly at about 90 sites across the US and Canada. More than 20 of these sites are within Class I areas. A 3-stage filter pack is used to measure nitrogen concentrations. Dry deposition flux is then calculated using the dry deposition velocity estimated by the Multi-Layer Model (CASTNET, 2014). For simplicity when discussing these values along with other observations, we refer to these derived quantities as dry deposition measurements, although we recognize here that dry deposition is not directly measured. We use monthly aggregate dry deposition of NH_4^+, NO_3^-, and HNO_3 for select sites. Yellowstone and Pinedale, WY, measurements are used for GT since there is no CASTNET site in GT.

2.2 Model description

GEOS-Chem (www.geos-chem.org) is a 3-dimensional atmospheric CTM driven by meteorological input from the Goddard Earth Observing System (GEOS) of the NASA Global Modeling and Assimilation Office (Bey et al., 2001). We use GEOS-Chem ad-

ACPD
15, 23089–23130, 2015

joint version 35 with a nested grid resolution of 1/2° latitude ×2/3° longitude with 47 vertical layers up to 0.01 hPa (Wang et al., 2004; Chen et al., 2009; Zhang et al., 2011) for the modeling domain over the contiguous US (126–66° W, 13–57° N). The model includes detailed tropospheric gas-phase chemistry of the O_3-NO_x-hydrocarbon system (Hudman et al., 2007). Aerosols are assumed to be externally mixed and the thermodynamic equilibrium between gases and aerosol of NH_3-H_2SO_4-HNO_3 is calculated using RPMARES (Park et al., 2004). Wet deposition includes sub-grid scavenging in convective updrafts, large scale in-cloud rainout, and below-cloud washout (Liu et al., 2001). Dry deposition is calculated using a resistance-in-series model (Wesely, 1989; Wang et al., 1998). Resistances are aerodynamic resistance, quasi-laminar sublayer resistance, and bulk surface resistance. Bulk surface resistances are specified by different surface type, i.e., vegetation types (Wesely, 1989). We use vegetation types from Olson (1992), shown in Fig. 1.

Anthropogenic emissions of NO_x, SO_2, and NH_3 in GEOS-Chem are taken from the National Emissions Inventory produced by the US EPA (EPA/NEI2008). Annual emissions of NO_x and NH_3 in the contiguous US in 2010 are shown in Table 1. Mobile emissions of NH_3 are not shown explicitly here, as they are $< 4\,\%$ of the US total in the NEI2008, although this may be an underestimate in urban areas (Kean et al., 2009). Anthropogenic sources of NO_x includes surface sources, electric generating units (EGUs), and non-EGU industrial point sources. Surface sources of NO_x comprises on-road (diesel and gasoline exhaust from cars and trucks, 68.4 %), non-road (off-road vehicles, construction equipment, industrial, commercial, and agricultural engines, 17.2 %), and non-point (not otherwise included, e.g., residential heating, oil and gas development, 14.4 %) sources. Biomass burning emissions are taken from the 3-h GFED3 inventory (Mu et al., 2011; van der Werf et al., 2010). NO_x emissions from aircraft are described in Wang et al. (1998). Natural emissions of NO_x are from lightning (Murray et al., 2012) and soil (Yienger and Levy, 1995; Wang et al., 1998). Natural emissions of NH_3 from soil, vegetation, and ocean sources are from the GEIA inventory (Bouwman et al., 1997). In Sect. 3.3, we consider NH_3 emissions constrained by

ACPD
15, 23089–23130, 2015

remote sensing observations from Zhu et al. (2013), which we refer to as optimized NEI2005.

2.3 Nr deposition metrics in Federal Class I areas

Here we consider several metrics (cost functions) for quantifying Nr deposition and CL exceedances in Federal Class I areas. The cost functions in this study include the following constituents: the sum of wet and dry deposition of NH_3, NH_4^+, NO_3^-, and HNO_3, and dry deposition of NO_2, PANs (peroxyacetyl nitrate and higher peroxyacyl nitrates: peroxymethacroyl nitrate, peroxypropionyl nitrate), alkyl nitrate, and N_2O_5. Although dry deposition of NO_2, PANs, alkyl nitrate, and N_2O_5 are not part of the CL estimates by Pardo et al. (2011), the sum of these species does not significantly contribute to our modeled Nr deposition or comparison to these CLs.

Strategies for reducing Nr deposition in Class I areas may consider the following questions. (1) Which emissions contribute the most to the spatial extent of Class I regions in exceedance? (2) What is the amount by which emissions contribute to the severity of Nr deposition on Class I areas above CLs? and (3) How do emissions from different source locations and sectors affect Nr deposition in different Class I areas?

Each of these three questions corresponds to unique approaches to defining the cost function for our sensitivity calculations. For the first question, the cost function, J_a [kg N ha^{-1} yr^{-1}], is the sum of Nr deposition in all Class I areas in CL exceedance, defined as

$$J_a = \sum_{i=1}^{L} \text{annDep}_i \beta_i, \quad (1)$$

where annDep_i is the annual Nr deposition in grid cell i, and β_i is the fraction of the grid cell i that is contained within a Class I area. L is the number of grid cells containing Federal Class I areas in which annual modeled Nr deposition has exceeded the CL values we use in this study. This metric is proportional to the total area of Class I

ACPD
15, 23089–23130, 2015

regions in CL exceedance. Sensitivities of J_a with resect to emissions thus identify which emissions contribute to the total spatial extent of Class I areas that have Nr deposition above their CL by any amount.

For the second question, the cost function, J_c [(kg N ha^{-1} yr^{-1})^2], is defined as

$$J_c = 0.5 \sum_{i=1}^{L} \alpha_i^2 \beta_i, \quad (2)$$

where $\alpha_i = \text{annDep}_i - \text{CL}_i$, and CL_i is the critical load in grid cell i. While both Eqs. (1) and (2) include only regions where annual Nr deposition is higher than the CL, Eq. (2) is more strongly related to the magnitude of the Nr deposition in exceedance (the factor of 0.5 is habitually included for sensitivity calculations based on the first derivative of J). Sensitivities of J_a reflect the contribution of emissions to the magnitude of Nr deposition above CL loads, which can then guide analysis of mitigation efforts for reducing the most severe levels of Nr deposition.

Lastly, a third cost function is formulated for case studies of specific individual Class I areas. It is defined as the annual Nr deposition in a region [kg N ha^{-1} yr^{-1}],

$$J_p = \sum_{i=1}^{N} \text{annDep}_i \beta_i, \quad (3)$$

where N is number of grid cells for which β_i is nonzero for an individual Class I area.

2.4 GEOS-Chem adjoint model

The GEOS-Chem adjoint model (Henze et al., 2007) is a tool for receptor-based inverse modeling and sensitivity analysis (e.g., Kopacz et al., 2009; Wecht et al., 2012; Zhu et al., 2013). When it is used for a sensitivity analysis, gradients of the cost function with respect to all model parameters are calculated simultaneously, making the model a very efficient tool for source attribution (e.g., Walker et al., 2012; Paulot et al., 2013;

ACPD
15, 23089–23130, 2015

Lapina et al., 2014; Lee et al., 2014). Here we use the model to evaluate the sensitivity of Nr deposition to emission sources, including for the first time all components of Nr present in the GEOS-Chem "full-chemistry" simulation.

Non-normalized sensitivities, which have units of the cost function per kg emission, quantify the efficiency of emissions' impact on Nr deposition. These are defined as

$$\lambda_{i,j} \equiv \frac{\partial J}{\partial E_{i,j}}, \tag{4}$$

where J is any of the cost functions defined in Sect. 2.3, and $\lambda_{i,j}$ is found from solution of the adjoint model. $E_{i,j}$ is the emission at grid cell i of species j. Details of the adjoint model description and validation have been presented previously (Henze et al., 2007, 2009). We also consider the semi-normalized sensitivity [kg N ha^{-1} yr^{-1}], defined as,

$$\chi_{i,j,k} \equiv \lambda_{i,j} \cdot E_{i,j,k}, \tag{5}$$

where $E_{i,j,k}$ is the emission at grid cell i of species j from sector k. This sensitivity linearly approximates the contribution to the cost function of the emission in location i, of species j, from sector k. While the adjoint model computes sensitivities with respect to all emissions (e.g., SO_2, VOCs, etc.), here we focus our analysis on sensitivities with respect to emissions of NH_3 and NO_x from anthropogenic and natural sources, which are the largest. Sensitivity calculations are performed monthly, including a one week spin-up for each month to capture the influence of emissions from the end of the previous month.

3 Results

3.1 Evaluation of simulated Nr deposition

Figure 2 shows the spatial distribution of total, reduced, and oxidized annual Nr deposition in the contiguous US in 2010 calculated with GEOS-Chem. Total consists of

ACPD
15, 23089–23130, 2015

all species included in the cost function, reduced is the sum of wet and dry deposition of NH_3 and NH_4^+, and oxidized is total minus reduced. Total Nr deposition ranges from 2 to 5 kg N ha^{-1} yr^{-1} in the West, except in some parts of California where is it > 12 kg N ha^{-1} yr^{-1}, and from 6 to 20 kg N ha^{-1} yr^{-1} in the East. Annual total Nr deposition over the contiguous US is 5.6 Tg N (3.2 oxidized, 2.4 reduced). Oxidized Nr is higher than reduced Nr overall, while reduced Nr is higher in mid-California, Iowa, and eastern North Carolina. The spatial distribution of reduced and oxidized Nr deposition is comparable with current (2011 and 2012 average) wet deposition measurement patterns analyzed by Du et al. (2014). However, Du et al. (2014) found greater wet deposition of NH_4^+ compared to NO_3^- over the contiguous US except in the Northeast region. The larger fraction of reduced Nr in their work may be related to increasing NH_3 and decreasing NO_x emissions and overestimated HNO_3 in the present study, as discussed below.

Zhang et al. (2012) previously estimated Nr deposition in the US using GEOS-Chem (oxidized: 4.2, reduced: 2.3 Tg N yr^{-1}). Our simulations have about 24 % less oxidized Nr deposition, and similar amounts of reduced Nr deposition. The simulations in Zhang et al. (2012) were for 2006 to 2008 and used emissions from the NEI2005 inventory, in which NO_x emissions are about 27 % higher and NH_3 emissions 10 % lower than those used in our study. Although the emissions are different, wet and dry HNO_3 and dry NO_3^- deposition from the two studies are very similar. Dry deposition of NO_2 and N_2O_5 in our results are smaller than Zhang et al. (2012), which is reasonable considering the differences in emissions. Zhang et al. (2012) found that modeled HNO_3 deposition is overestimated when isoprene nitrate is not explicitly treated but deposits as HNO_3, as it does in our simulation. Further, comparison of modeled to measured HNO_3 in Zhang et al. (2012) required consideration of sub-grid concentration gradients near the surface, and ambient HNO_3 concentrations are overestimated (Heald et al., 2012), possibly owing to excessive N_2O_5 hydrolysis. This suggests that oxidized Nr may be overestimated in our study. Schwede and Lear (2014) also made an effort to provide spatially continuous information of Nr deposition using a hybrid method

ACPD
15, 23089–23130, 2015

to combine comprehensive measurements and modeled data. They generated maps of Nr deposition for total, reduced, and oxidized Nr, for multiple years including 2010. In comparison to their total Nr deposition map, our result shows good agreement in terms of magnitude and spatial distribution for 2010, except in the central mountain regions where Schwede and Lear (2014) shows noticeable higher Nr deposition owing to higher dry deposition of reduced Nr.

For the eight selected Class I areas, we first compare seasonal average values from measurements provided by NADP/NTN and CASTNET versus GEOS-Chem model estimates (Fig. 3). Total simulated Nr deposition (J_p) is also plotted in Fig. 3 as blue diamonds to show the role of non-measured species. Seasonal averages are calculated from monthly values. Measured species correspond to the sum of modeled wet NH_3, NH_4^+, HNO_3, and NO_3^-, and dry NH_4^+, NO_3^-, and HNO_3. The squared correlation coefficient (R^2) is shown in each plot. For SQ, R^2 is calculated with spring, fall, and winter data. The model well reproduces the seasonality of measurements ($R^2 > 0.6$) except at JT. Low correlation in JT is due to the model underestimation of winter deposition which will be further discussed in the next paragraph. For all sites, measurements and model estimates have maximum values in the summer. Seasonally averaged measurement values range from 0 to 0.6 kg N ha^{-1} month^{-1} (monthly value 0–1.3 kg N ha^{-1} month^{-1}), model estimates range from 0.0 to 1.2 kg N ha^{-1} month^{-1} (monthly value 0–1.3 kg N ha^{-1} month^{-1}) and J_p range from 0.1 to 1.3 kg N ha^{-1} month^{-1} (monthly value 0–1.4 kg N ha^{-1} month^{-1}). Our model estimates is also higher than the measurement in the spring and summer in SM and SD, likely owing to overestimated HNO_3 as discussed above. Schwede and Lear (2014) shows more than two times higher total annual Nr deposition in RM compared to our result. This discrepancy is largely owing to differences in model estimated of dry deposition of NH_3 which are not measured. In addition, Hicks (2006) found that measurements of HNO_3 dry deposition in clearings, such as the CASTNET sites in SD and SM from which dry deposition measurements are derived, are lower than mea-

ACPD
15, 23089–23130, 2015

surements of dry deposition to the surrounding forest canopy. This may also contribute to the discrepancy between the model and the measurement shown in this study.

Figure 4 shows the model speciation of J_p. Non-measured species are dry deposition of NO_2, PANs, alkyl nitrate, N_2O_5 (lumped as others in Fig. 4) and dry NH_3. Non-measured species account for 0.5 % (winter, SM) to 55.6 % (summer, SQ) of seasonally averaged J_p values in the model. Dry deposition of NH_3 accounts for 14 % of total annual Nr deposition. The summer maximum of J_p is mainly driven by wet deposition of HNO_3 (VY, SM, SD, BB, RM) and dry deposition of HNO_3 (VY, GT, JT, SQ). Dry deposition of NH_3 is a major contributor in SQ. Organics make only a small contribution (< 5 %) to Nr deposition in the model. While it is known that organics account for $\sim$ 30 % of total Nr deposition (Neff et al., 2002; Cornell, 2011), we expect organics to underestimated in our model because only dry deposition is included for these species and isoprene nitrate is not explicitly treated (Zhang et al., 2012).

Annual modeled Nr deposition (J_p) ranges from 2.2 to 10.7 kg N ha^{-1} yr^{-1}, and is highest in SD and SM and lowest in BB. The dotted lines in Fig. 3 show the annual CLs from Ellis et al. (2013) divided by twelve. VY, SM, SD, RM, GT, and SQ are considered to be in CL exceedance on an annual basis. Within California, annual Nr deposition in SQ is about 70 % larger than that in JT. This is influenced by the position of these parks relative to large upwind anthropogenic sources, as well as different vegetation types of the two parks (Fig 1). JT is 80 % desert where very low Nr is expected; in contrast, SQ has narrow conifers and mediterranean scrub. The lowest annual Nr deposition in BB is explained, in part, by the large fraction of desert (60 %) and succulent and thorn scrub (18 %); it is also far from large anthropogenic sources.

3.2 Source attribution using GEOS-Chem adjoint

3.2.1 Spatial and sectoral footprints of Nr deposition

The sensitivity of total annual Nr deposition (J_p) to emission sources is calculated by the GEOS-Chem adjoint model. The results can be understood as the contribution of

ACPD
15, 23089–23130, 2015

emissions in each grid cell to the Nr deposition in each Class I area. Figure 5 shows spatial distributions of the sensitivities of Nr deposition to NO_x and NH_3 emissions – the so called source footprint – for each region. Inset numbers are the annual Nr deposition in each area from all sources (J_p). Pie charts show the relative contributions to this value from specific emission sectors (sectors contributing < 1 % are not shown).

The source attribution results show significant variability in terms of the sectors contributing to Nr deposition in different Class I areas. Livestock NH_3 and surface source NO_x, i.e., mobile sources, are the major sources of Nr deposition, contributing more than 65 % to SM, SD, RM, GT, JT, and SQ. Livestock NH_3 contributions are largest for SQ (54 %) and smallest for BB (15 %). Mobile NO_x is the major emission source for JT (63 %), SM (40 %) and SD (38 %). Fertilizer NH_3 is the third most important source of Nr deposition for VY (14 %), GT (11 %), and SQ (8 %). In contrast to the other sites, for BB the contribution of natural sources of Nr (the sum of natural NH_3, lightning and soil NO_x equal to 47 %) is comparable to that of anthropogenic contributions. NO_x from EGUs is the third most important source for RM (12 %) and SD (9 %). Lightning is a considerable source not only for BB but for SM (9 %). Aircraft emissions have a noticeable impact only for JT (2 %).

Additional analysis was performed for RM, given the prevalence of studies on Nr deposition in this area. Figure 6 shows the source distributions of oxidized and reduced Nr. Our results suggest reduced Nr originates primarily from east of the park, while in contrast a large fraction of oxidized Nr originates from west of park. This is consistent with the spatial distributions of NH_3 versus NO_x emissions in the area surrounding the park. The high sensitivity of reduced Nr to sources west of RM in California and Idaho agrees with other recent studies (Benedict et al., 2013b; Malm et al., 2013; Thompson et al., 2015).

The results of the adjoint sensitivity calculations show that the spatial footprint of emissions affecting different Class I regions can vary by several hundred kilometers. Even though NO_x and NH_3, by themselves, have very short lifetimes (< 1 day), in the form of aerosol species they can influence Nr deposition over quite large distances,

ACPD
15, 23089–23130, 2015

which is reflected in the maps in Fig. 5. To provide a quantitative means of evaluating the spatial extent of the footprint for each region, Fig. 7 shows cumulative contributions of annual average monthly Nr deposition by radial distance from each site. Blue and red lines indicate distances for which the cumulative influence is 50 and 90 % of the total, respectively. For reference, the greatest distance within the contiguous US, from Florida to Washington, is about 4500 km. It can be inferred from the shape of the plot that VY, SM, and BB have broad source regions spreading ~ 1500 km from the site. In contrast, JT and SQ are mostly (90 %) influenced by sources within 700 km (JT) and 400 km (SQ). Local sources (within 50 km) contribute more than 20 % of total Nr deposition for SD, while the rest are from more distant regions spread across ~ 1100 km. For RM and GT, there is a jump in the cumulative distribution around 1200 km which is due to sources in California. Steep initial rises for JT and SQ correspond to the influence of local urban centers (Los Angeles and San Francisco, respectively).

3.2.2 Efficiency of emission impacts on Nr deposition

For each park, we also calculate the expected changes in Nr deposition (J_p) per kg emissions of NH_3-N, NO_x-N, and SO_2-S (i.e., the absolute sensitivities calculated with Eq. 4) in each month. These are a measure of transport efficiency of each species, largely determined by meteorology and aerosol partitioning. Figure 8 shows a few select results with unique seasonal features and Fig. 9 shows wind-roses in JJA and DJF for the select cases.

In JT, there is a clear seasonal trend (Fig. 8a). Nr deposition in the park is impacted most efficiently by sources in the NW-SE direction during the summer and by sources in the NE–SW direction in the winter, owing to changes in wind patterns (see Fig. 9, top). In RM, Nr deposition is owing to the sources from California during the summer, whereas the source footprints are much more localized during the winter (Fig. 8b). While stronger winds ($\geq 6\,m\,s^{-1}$) are actually more frequent in the winter (Fig. 9, middle), larger NH_3 emissions in the summer facilitate formation of NH_4NO_3 and thus long-range Nr transport. In SD, NH_3 emissions make a positive contribution to Nr deposition

ACPD
15, 23089–23130, 2015

during the summer, while emissions north of the park contribute negatively during the winter (Fig. 8c). These negative sensitivities occur because NH_4NO_3 formation is limited by NH_3 in the winter in SD. Thus, emissions of NH_3 contribute to formation of NH_4NO_3, which in turn has a longer lifetime in the atmosphere than gas-phase NH_3 or HNO_3. Consequently, Nr deposits far beyond the park leading to negative sensitivities for NH_3 emissions. This tradeoff is also manifested by SO_2 emissions having positive sensitivities during winter and negative sensitivities during summer. In NH_3 limited conditions (winter), increased SO_2 emissions would tie up NH_3 as aerosol $(NH_4)_2SO_4$ or NH_4HSO_4, leaving less NH_3 available to form NH_4NO_3.

3.2.3 Analysis of all Class I areas in critical load exceedance

CL exceedance in Class I areas are shown in Fig. 10. In order to see the number of grid cells in CL exceedance, the area of the regions are not reflected in this map; they are shown as filled cells if the fraction that the region occupies in the cell is greater than zero (although fractional grid cell areas, β_i, are considered in the model simulations themselves). The West/East contrast is clear. The number of cells in CL exceedance is larger in the West while the magnitude of the CL exceedance is larger in the East. This is not surprising considering the spatial distribution of Nr deposition (Fig. 2) and Class I areas. Among the 149 Class I areas in the contiguous US only 38 are located in the East. Figure 11a shows the sensitivity of J_a to NO_x and NH_3 emissions. This sensitivity indicates the regions where reducing emission will result in the largest decrease in the extent of Class 1 areas in CL exceedance. Figure 11b is the sensitivity of J_c to emissions. This sensitivity shows the sources that are causing the largest values of Nr deposition, relative to the CLs (i.e., excessive or severe values).

Comparison of the two types of sensitivity analysis suggests how different emissions control strategies might be considered to meet different objectives. Decreasing Nr emissions in California and regions surrounding RM and SM would be useful for reducing both the extent of Class I areas in CL exceedance and the amount of excessive Nr in Class I areas. Nr originating from Idaho, Utah, Washington, and Arizona contribute

ACPD
15, 23089–23130, 2015

more to the former, but less to the latter, as the Nr deposition in these regions is not as excessive as it is in other regions, as shown in Fig. 10. Reducing Nr emissions from the tip of Florida would reduce the area of regions in CL exceedance, while reductions to emissions in this area are not as beneficial for avoiding excessively high deposition, as this region has the highest CL (5 kg N ha^{-1} yr^{-1}) of those considered here.

For reduction of excessive Nr above the CL, sources with the largest impact are located in the East (i.e., Tennessee, Alabama, and Georgia) and the San Joaquin Valley in California. Interestingly, the distribution of contributions across sectors is similar for both J_a and J_c; surface NO_x and livestock NH_3 are the major emission sectors contributing to both the extent and severity of CL exceedances.

3.3 Uncertainty caused by NH_3 emissions

NH_3 emissions are known to have large uncertainties (e.g., Heald et al., 2012), more than a factor of two in total US emissions in some seasons (Henze et al., 2009; Paulot et al., 2014). To evaluate the robustness of our source attribution analysis with respect to NH_3 emissions uncertainties we compare our base case results using NEI2008 emissions to sensitivity results using NEI2005 NH_3 emissions optimized using remote sensing observations (Shephard et al., 2011) from Zhu et al. (2013). This is of interest not only because the magnitude of NH_3 emissions may change the contribution of NH_3 to Nr deposition, but also because Nr deposition is sensitive to long-range transport of ammonium and nitrate aerosol and NH_3 abundance exerts a strong, nonlinear, influence on nitrate partitioning. As shown in Zhu et al. (2013), in the optimized NEI2005 the overall NH_3 emissions have increased compared to the original NEI2005 inventory; emissions in California, the central US, and the Midwest are especially enhanced. Figure 12 shows the NH_3 emissions from the optimized NEI2005 and those used in this study, NEI2008. The NEI2008 inventory has even larger NH_3 emissions over the Midwest compared to the optimized NEI2005 in all three months shown here. In July, NH_3 emissions in the central US (Kansas, Nebraska, eastern Colorado, and Texas) and Washington are higher with the optimized NEI2005.

ACPD
15, 23089–23130, 2015

Case studies are performed for VY, SD, and RM, whose Nr deposition footprint (Fig. 5) includes regions showing noticeable differences between the two NH_3 emission inventories (Fig. 12). The non-normalized sensitivity, $\lambda_{i,j}$, remains constant with the changes in emissions but the semi-normalized sensitivity, $\chi_{i,j,k}$, is perturbed by the differences in $E_{i,j,k}$. Figure 13 shows the sensitivities of J_p to NH_3 emissions for these sites. Overall, when using NEI2008 the contribution of NH_3 emissions to J_p is larger than when using the optimized NEI2005 inventory in all cases. Differences in NH_3 emissions clearly affect sensitivities in VY. Differences in Minnesota and Iowa are mainly reflected in the sensitivities for Nr deposition in VY. The source footprint for this site gradually accumulates to 90 % of the total Nr deposition by 1700 km (see Figs. 5 and 7), which easily encompasses the perturbed regions in Iowa that are at most ~ 840 km away. SD is not affected much by different NH_3 inventories in most seasons, as 50 % of total Nr deposition is owing to sources within 250 km (Fig. 7), where the emissions inventories are similar, except in April, where NEI2008 leads to broader estimates of the source footprints. Local influences become more pronounced for SD in the footprints estimated using the NEI2005 emissions. For the base case, Nr deposition was found to have significant long range influences for RM. However, when using the optimized NEI2005 emissions, where NH_3 sources in eastern Colorado are estimated to be much larger, the relative role of long-range influence from east of the park is reduced.

4 Discussion and conclusions

We used the GEOS-Chem CTM and its adjoint model for Nr deposition source attribution in Federal Class I areas in the US. First, modeled Nr deposition is compared with NADP/NTN (NADP, 2015) and CASTNET (CASTNET, 2014) measurements and other modeling studies (Zhang et al., 2012; Schwede and Lear, 2014). The seasonality of measured species is generally well represented by the model ($R^2 > 0.6$), except in Joshua Tree. Modeled Nr deposition contains large contributions from wet HNO_3 which

ACPD
15, 23089–23130, 2015

is likely overestimated in the version of the model used here (Zhang et al., 2012), leading to overestimates of Nr deposition in Smoky Mountain and Shenandoah of up to 0.6 kg N ha^{-1} $month^{-1}$. Still, adequate model performance in other seasons and locations suggests a considerable contribution of dry deposition of NH_3 in some locations and seasons, consistent with Schwede and Lear (2014). A significant fraction of Nr deposition in the central mountain region (including Rocky Mountain National Park) is estimated to be in the form of reduced nitrogen, similar to several other recent studies (Benedict et al., 2013b; Malm et al., 2013; Thompson et al., 2015), although such estimates are to model uncertainties in NH_3 emissions and modeled NO_3^-. Among the eight selected Class I areas, Voyageurs, Smoky Mountain, Shenandoah, Rocky Mountain, Grand Teton, and Sequoia are estimated to be in exceedance of the most conservative estimates of CLs from Pardo et al. (2011).

The spatial distribution of annual Nr deposition sources are investigated using the adjoint of GEOS-Chem. NH_3 emissions from livestock and NO_x emissions from mobile sources are the major sectors that contribute to Nr deposition in all selected Class I areas, except Big Bend where natural sources contribute comparably with anthropogenic sources. Nr deposition in Joshua Tree and Sequoia, both located in California, tends to originate from local (< 700 km) sources, whereas Nr deposition in the mountain regions (Grand Teton and Rocky Mountain) are ~ 50 % from nearby sources (< 400 km) and the rest from sources as far away as California (~ 1300 km). For other parks (Voyageurs, Smoky Mountain, Shenandoah, and Big Bend), sources are broadly distributed radially. Overall, these results suggest that mitigating Nr deposition in many specific areas may require substantial consideration of interstate transport.

The efficiency of emissions to impact Nr deposition is evaluated at the per-kg emission level for NH_3-N, NO_x-N, and SO_2-S. This result represents the response of Nr deposition to additional emissions, which is useful for consideration of the impact of future emission, such as those for NH_3 emissions that are expected to increase in the future due to increased agricultural activities (Moss et al., 2010). In Joshua Tree, NH_3 emission efficiencies show distinct seasonality in terms of their locations. The NW-SE

ACPD
15, 23089–23130, 2015

impact is strongest in summer and the NE-SW impact is dominant in winter. In Rocky Mountain, effective regions are broader in the summer even though stronger winds are more frequent in the winter, owing to to larger NH_3 sources in the summer. In Shenandoah, NH_3 emissions to the north of the park inhibit Nr deposition in the park during the winter. This response is interesting, and explainable from consideration of aerosol partitioning and transport, although the absolute significance is not that large owing to the small levels of deposition here in the winter.

Sources of Nr deposition in all Class I areas in CL exceedance throughout the US are studied using two approaches: emissions that increase the total area of Class I areas that are in CL exceedance and emissions that increase the magnitude of the excessive Nr deposition above CLs. Our result suggests that on of the largest source regions contributing to the spatial extent of Class I regions in CL exceedance is California. On the other hand, Nr sources in the Eastern US, i.e., Tennessee, Alabama, and Georgia, in addition to California, contribute the most to excessive Nr above the CL in Class I areas. Thus, strategies for reducing the spatial extent of ecological damage from excessive Nr deposition may differ from those aimed at reducing its severity.

Lastly, case studies are performed for Voyageurs, Shenandoah, and Rocky Mountain national parks using different NH_3 emission inventories, which have large uncertainties, in order to evaluate how sensitive our source footprint estimates are to underlying model emissions. We adopted NH_3 emissions optimized using remote sensing observations (Zhu et al., 2013) to compare with our results using the NEI2008 inventory, which has greater NH_3 emissions in the Midwest and California. Difference in semi-normalized sensitivity is most apparent in April and July. Differences of NH_3 emissions in Minnesota and Iowa are mainly reflected in the source footprint for Voyageurs. Estimated local influences become more important for Shenandoah when using the optimized NEI2005 inventory. For Rocky Mountain, when using the optimized NEI2005 emissions, NH_3 sources in eastern Colorado are estimated to be much larger, but the role of long-range influences is reduced.

ACPD
15, 23089–23130, 2015

Overall, the results presented here provide useful information for considering how emissions control strategies both regionally and nationally may impact Nr deposition in Federal Class I areas. Future work may strive to apply such methods to higher resolution models, as model resolution may impact the ability to resolve fine-scale features delineating specific sources or areas of influence and complex topography in Class I areas. In addition, considering the role of bi-directional NH_3 exchange (e.g., Zhu et al., 2015), which can effectively extend the source footprint owing to reemission of NH_3 from NH_3 rich soils, would be of interest. Lastly, as source attribution estimates for Nr deposition are intrinsically sensitive to uncertainties in the balance of emissions between NH_3 and NO_x, even if the total Nitrogen emissions are correct, further effort should be made to improve knowledge of the distributions and trends in NH_3 and NO_x emissions.

Acknowledgements. We acknowledge support from the NASA Air Quality Applied Sciences Team, grant NNX11AI54G and NSF grant ANT 1244958.

References

Benedict, K. B., Chen, X., Sullivan, A. P., Li, Y., Day, D., Prenni, A. J., Levin, E. J. T., Kreidenweis, S. M., Malm, W. C., Schichtel, B. A., and Collett, J. L.: Atmospheric concentrations and deposition of reactive nitrogen in Grand Teton National Park, J. Geophys. Res. Atmos., 118, 11875–11887, doi:10.1002/2013JD020394, 2013a. 23092

Benedict, K. B., Day, D., Schwandner, F. M., Kreidenweis, S. M., Schichtel, B., Malm, W. C., and Collett Jr., J. L.: Observations of atmospheric reactive nitrogen species in Rocky Mountain National Park and across northern Colorado, Atmos. Environ., 64, 66–76, doi:10.1016/j.atmosenv.2012.08.066, 2013b. 23102, 23107

Bey, I., Jacob, D. J., Yantosca, R. M., Logan, J. A., Field, B. D., Fiore, A. M., Li, Q., Liu, H. Y., Mickley, L. J., and Schultz, M. G.: Global modeling of tropospheric chemistry with assimilated meteorology: Model description and evaluation, J. Geophys. Res., 106, 23073–23095, doi:200110.1029/2001JD000807, 2001. 23094

ACPD
15, 23089–23130, 2015

Bobbink, R., Hicks, K., Galloway, J., Spranger, T., Alkemade, R., Ashmore, M., Bustamante, M., Cinderby, S., Davidson, E., Dentener, F., Emmett, B., Erisman, J.-W., Fenn, M., Gilliam, F., Nordin, A., Pardo, L., and De Vries, W.: Global assessment of nitrogen deposition effects on terrestrial plant diversity: a synthesis, Ecol. Appl., 20, 30–59, doi:10.1890/08-1140.1, 2010. 23091

Bouwman, A. F., Lee, D. S., Asman, W. a. H., Dentener, F. J., Van Der Hoek, K. W., and Olivier, J. G. J.: A global high-resolution emission inventory for ammonia, Global Biogeochem. Cy., 11, 561–587, doi:10.1029/97GB02266, 1997. 23095

Bowman, W. D., Murgel, J., Blett, T., and Porter, E.: Nitrogen critical loads for alpine vegetation and soils in Rocky Mountain National Park, J. Environ. Manage., 103, 165–171, doi:10.1016/j.jenvman.2012.03.002, 2012. 23092

CASTNET: US Environmental Protection Agency Clean Air Markets Division Clean Air Status and Trends Network (CASTNET) Data table accessed (NH_4, NO_3, HNO_3 Weekly Dry Deposition), available at: www.epa.gov/castnet, last access: 9 November, 2014. 23094, 23106

Chen, D., Wang, Y., McElroy, M. B., He, K., Yantosca, R. M., and Le Sager, P.: Regional CO pollution and export in China simulated by the high-resolution nested-grid GEOS-Chem model, Atmos. Chem. Phys., 9, 3825–3839, doi:10.5194/acp-9-3825-2009, 2009. 23095

Clark, C. M., Morefield, P. E., Gilliam, F. S., and Pardo, L. H.: Estimated losses of plant biodiversity in the United States from historical N deposition (1985–2010), Ecology, 94, 1441–1448, doi:10.1890/12-2016.1, 2013. 23091

Cornell, S. E.: Atmospheric nitrogen deposition: Revisiting the question of the importance of the organic component, Environ. Pollut., 159, 2214–2222, doi:10.1016/j.envpol.2010.11.014, 2011. 23101

Du, E., Vries, W. d., Galloway, J. N., Hu, X., and Fang, J.: Changes in wet nitrogen deposition in the United States between 1985 and 2012, Environ. Res. Lett., 9, 095004, doi:10.1088/1748-9326/9/9/095004, 2014. 23099

Duce, R. A., LaRoche, J., Altieri, K., Arrigo, K. R., Baker, A. R., Capone, D. G., Cornell, S., Dentener, F., Galloway, J., Ganeshram, R. S., Geider, R. J., Jickells, T., Kuypers, M. M., Langlois, R., Liss, P. S., Liu, S. M., Middelburg, J. J., Moore, C. M., Nickovic, S., Oschlies, A., Pedersen, T., Prospero, J., Schlitzer, R., Seitzinger, S., Sorensen, L. L., Uematsu, M., Ulloa, O., Voss, M., Ward, B., and Zamora, L.: Impacts of Atmospheric Anthropogenic Nitrogen on the Open Ocean, Science, 320, 893–897, doi:10.1126/science.1150369, 2008. 23091

ACPD
15, 23089–23130, 2015

Ellis, R. A., Jacob, D. J., Sulprizio, M. P., Zhang, L., Holmes, C. D., Schichtel, B. A., Blett, T., Porter, E., Pardo, L. H., and Lynch, J. A.: Present and future nitrogen deposition to national parks in the United States: critical load exceedances, Atmos. Chem. Phys., 13, 9083–9095, doi:10.5194/acp-13-9083-2013, 2013. 23092, 23093, 23101

Fenn, M. E., Baron, J. S., Allen, E. B., Rueth, H. M., Nydick, K. R., Geiser, L., Bowman, W. D., Sickman, J. O., Meixner, T., Johnson, D. W., and Neitlich, P.: Ecological Effects of Nitrogen Deposition in the Western United States, BioScience, 53, 404–420, doi:10.1641/0006-3568(2003)053[0404:EEONDI]2.0.CO;2, 2003. 23091

Fenn, M. E., Allen, E. B., Weiss, S. B., Jovan, S., Geiser, L. H., Tonnesen, G. S., Johnson, R. F., Rao, L. E., Gimeno, B. S., Yuan, F., Meixner, T., and Bytnerowicz, A.: Nitrogen critical loads and management alternatives for N-impacted ecosystems in California, J. Environ. Manage., 91, 2404–2423, doi:10.1016/j.jenvman.2010.07.034, 2010. 23092

Galloway, J. N., Aber, J. D., Erisman, J. W., Seitzinger, S. P., Howarth, R. W., Cowling, E. B., and Cosby, B. J.: The nitrogen cascade, BioScience, 53, 341–356, doi:10.1641/0006-3568(2003)053[0341:TNC]2.0.CO;2, 2003. 23091

Gruber, N. and Galloway, J. N.: An Earth-system perspective of the global nitrogen cycle, Nature, 451, 293–296, doi:10.1038/nature06592, 2008. 23091

Heald, C. L., Collett Jr., J. L., Lee, T., Benedict, K. B., Schwandner, F. M., Li, Y., Clarisse, L., Hurtmans, D. R., Van Damme, M., Clerbaux, C., Coheur, P.-F., Philip, S., Martin, R. V., and Pye, H. O. T.: Atmospheric ammonia and particulate inorganic nitrogen over the United States, Atmos. Chem. Phys., 12, 10295–10312, doi:10.5194/acp-12-10295-2012, 2012. 23099, 23105

Henze, D. K., Hakami, A., and Seinfeld, J. H.: Development of the adjoint of GEOS-Chem, Atmos. Chem. Phys., 7, 2413–2433, doi:10.5194/acp-7-2413-2007, 2007. 23097, 23098

Henze, D. K., Seinfeld, J. H., and Shindell, D. T.: Inverse modeling and mapping US air quality influences of inorganic $PM_{2.5}$ precursor emissions using the adjoint of GEOS-Chem, Atmos. Chem. Phys., 9, 5877–5903, doi:10.5194/acp-9-5877-2009, 2009. 23092, 23098, 23105

Hicks, B. B.: Dry deposition to forests – On the use of data from clearings, Agricultural and Forest Meteorology, 136, 214–221, doi:10.1016/j.agrformet.2004.06.013, 2006. 23100

Hudman, R. C., Jacob, D. J., Turquety, S., Leibensperger, E. M., Murray, L. T., Wu, S., Gilliland, A. B., Avery, M., Bertram, T. H., Brune, W., Cohen, R. C., Dibb, J. E., Flocke, F. M., Fried, A., Holloway, J., Neuman, J. A., Orville, R., Perring, A., Ren, X., Sachse, G. W., Singh, H. B., Swanson, A., and Wooldridge, P. J.: Surface and lightning sources of nitrogen oxides over

ACPD
15, 23089–23130, 2015

the United States: Magnitudes, chemical evolution, and outflow, J. Geophys. Res. Atmos., 112, D12S05, doi:10.1029/2006JD007912, 2007. 23095

Kean, A. J., Littlejohn, D., Ban-Weiss, G. A., Harley, R. A., Kirchstetter, T. W., and Lunden, M. M.: Trends in on-road vehicle emissions of ammonia, Atmos. Environ., 43, 1565–1570, doi:10.1016/j.atmosenv.2008.09.085, 2009. 23095

Kopacz, M., Jacob, D. J., Henze, D. K., Heald, C. L., Streets, D. G., and Zhang, Q.: Comparison of adjoint and analytical Bayesian inversion methods for constraining Asian sources of carbon monoxide using satellite (MOPITT) measurements of CO columns, J. Geophys. Res., 114, D04305, doi:10.1029/2007JD009264, 2009. 23097

Lapina, K., Henze, D. K., Milford, J. B., Huang, M., Lin, M., Fiore, A. M., Carmichael, G., Pfister, G. G., and Bowman, K.: Assessment of source contributions to seasonal vegetative exposure to ozone in the US, J. Geophys. Res. Atmos., 119, 324–340, doi:10.1002/2013JD020905, 2014. 23098

Lee, H.-M., Henze, D. K., Alexander, B., and Murray, L. T.: Investigating the sensitivity of surface-level nitrate seasonality in Antarctica to primary sources using a global model, Atmos. Environ., 89, 757–767, doi:10.1016/j.atmosenv.2014.03.003, 2014. 23098

Liu, H., Jacob, D. J., Bey, I., and Yantosca, R. M.: Constraints from 210Pb and 7Be on wet deposition and transport in a global three-dimensional chemical tracer model driven by assimilated meteorological fields, J. Geophys. Res. Atmos., 106, 12109–12128, doi:10.1029/2000JD900839, 2001. 23095

Malm, W. C., Schichtel, B. A., Barna, M. G., Gebhart, K. A., Rodriguez, M. A., Jr, J. L. C., Carrico, C. M., Benedict, K. B., Prenni, A. J., and Kreidenweis, S. M.: Aerosol species concentrations and source apportionment of ammonia at Rocky Mountain National Park, J. Air Waste Manage., 63, 1245–1263, doi:10.1080/10962247.2013.804466, 2013. 23102, 23107

Moss, R. H., Edmonds, J. A., Hibbard, K. A., Manning, M. R., Rose, S. K., van Vuuren, D. P., Carter, T. R., Emori, S., Kainuma, M., Kram, T., Meehl, G. A., Mitchell, J. F. B., Nakicenovic, N., Riahi, K., Smith, S. J., Stouffer, R. J., Thomson, A. M., Weyant, J. P., and Wilbanks, T. J.: The next generation of scenarios for climate change research and assessment, Nature, 463, 747–756, doi:10.1038/nature08823, 2010. 23107

Mu, M., Randerson, J. T., van der Werf, G. R., Giglio, L., Kasibhatla, P., Morton, D., Collatz, G. J., DeFries, R. S., Hyer, E. J., Prins, E. M., Griffith, D. W. T., Wunch, D., Toon, G. C., Sherlock, V., and Wennberg, P. O.: Daily and 3-hourly variability in global fire emissions and

ACPD
15, 23089–23130, 2015

consequences for atmospheric model predictions of carbon monoxide, J. Geophys. Res., 116, D24303, doi:10.1029/2011JD016245, 2011. 23095
Murray, L. T., Jacob, D. J., Logan, J. A., Hudman, R. C., and Koshak, W. J.: Optimized regional and interannual variability of lightning in a global chemical transport model constrained by LIS/OTD satellite data, J. Geophys. Res. Atmos., 117, D20307, doi:10.1029/2012JD017934, 2012. 23095
NADP: National Atmospheric Deposition Program (NRSP-3), NADP Program Office, Illinois State Water Survey, 2204 Griffith Dr., Champaign, IL, USA, 2015. 23094, 23106
Neff, J. C., Holland, E. A., Dentener, F. J., McDowell, W. H., and Russell, K. M.: The origin, composition and rates of organic nitrogen deposition: A missing piece of the nitrogen cycle?, Biogeochemistry, 57–58, 99–136, doi:10.1023/A:1015791622742, 2002. 23101
Nilsson, J.: Critical Loads for Sulphur and Nitrogen, in: Air Pollution and Ecosystems, edited by: Mathy, P., 85–91, Springer, the Netherlands, doi:10.1007/978-94-009-4003-1_11, 1988. 23091
Olson, J. S.: Digital raster data on a 10 minute geographic 1080 × 2160 grid in Global Ecosystems Database, version 1.0, Disc A, edited by: NOAA Natl. Geophys. Data Center, Boulder, CO, USA, 1992. 23095, 23118
Pardo, L. H., Fenn, M. E., Goodale, C. L., Geiser, L. H., Driscoll, C. T., Allen, E. B., Baron, J. S., Bobbink, R., Bowman, W. D., Clark, C. M., Emmett, B., Gilliam, F. S., Greaver, T. L., Hall, S. J., Lilleskov, E. A., Liu, L., Lynch, J. A., Nadelhoffer, K. J., Perakis, S. S., Robin-Abbott, M. J., Stoddard, J. L., Weathers, K. C., and Dennis, R. L.: Effects of nitrogen deposition and empirical nitrogen critical loads for ecoregions of the United States, Ecol. Appl., 21, 3049–3082, doi:10.1890/10-2341.1, 2011. 23091, 23093, 23096, 23107
Park, R. J., Jacob, D. J., Field, B. D., Yantosca, R. M., and Chin, M.: Natural and transboundary pollution influences on sulfate-nitrate-ammonium aerosols in the United States: Implications for policy, J. Geophys. Res., 109, D15204, doi:10.1029/2003JD004473, 2004. 23095
Paulot, F., Jacob, D. J., and Henze, D. K.: Sources and processes contributing to nitrogen deposition: an adjoint model analysis applied to biodiversity hotspots worldwide, Environ. Sci. Technol., 47, 3226–3233, doi:10.1021/es3027727, 2013. 23092, 23097
Paulot, F., Jacob, D. J., Pinder, R. W., Bash, J. O., Travis, K., and Henze, D. K.: Ammonia emissions in the United States, European Union, and China derived by high-resolution inversion of ammonium wet deposition data: Interpretation with a new agricultural emissions inventory

ACPD
15, 23089–23130, 2015

(MASAGE_NH3), J. Geophys. Res. Atmos., 119, 4343–4364, doi:10.1002/2013JD021130, 2014. 23105

Reay, D. S., Dentener, F., Smith, P., Grace, J., and Feely, R. A.: Global nitrogen deposition and carbon sinks, Nature Geosci., 1, 430–437, doi:10.1038/ngeo230, 2008. 23091

Sala, O. E., Chapin, F. S., Iii, Armesto, J. J., Berlow, E., Bloomfield, J., Dirzo, R., Huber-Sanwald, E., Huenneke, L. F., Jackson, R. B., Kinzig, A., Leemans, R., Lodge, D. M., Mooney, H. A., Oesterheld, M., Poff, N. L., Sykes, M. T., Walker, B. H., Walker, M., and Wall, D. H.: Global biodiversity scenarios for the year 2100, Science, 287, 1770–1774, doi:10.1126/science.287.5459.1770, 2000. 23091

Schwede, D. B. and Lear, G. G.: A novel hybrid approach for estimating total deposition in the United States, Atmos. Environ., 92, 207–220, doi:10.1016/j.atmosenv.2014.04.008, 2014. 23099, 23100, 23106, 23107

Shephard, M. W., Cady-Pereira, K. E., Luo, M., Henze, D. K., Pinder, R. W., Walker, J. T., Rinsland, C. P., Bash, J. O., Zhu, L., Payne, V. H., and Clarisse, L.: TES ammonia retrieval strategy and global observations of the spatial and seasonal variability of ammonia, Atmos. Chem. Phys., 11, 10743–10763, doi:10.5194/acp-11-10743-2011, 2011. 23105

Stevens, C. J., Dise, N. B., Mountford, J. O., and Gowing, D. J.: Impact of nitrogen deposition on the species richness of grasslands, Science, 303, 1876–1879, doi:10.1126/science.1094678, 2004. 23091

Sullivan, T. J., Cosby, B. J., Tonnessen, K. A., and Clow, D. W.: Surface water acidification responses and critical loads of sulfur and nitrogen deposition in Loch Vale watershed, Colorado, Water Resour. Res., 41, W01021, doi:10.1029/2004WR003414, 2005. 23091

Thompson, T. M., Rodriguez, M. A., Barna, M. G., Gebhart, K. A., Hand, J. L., Day, D. E., Malm, W. C., Benedict, K. B., Collett, J. L., and Schichtel, B. A.: Rocky Mountain National Park reduced nitrogen source apportionment: RMNP NITROGEN SOURCE APPORTIONMENT, J. Geophys. Res. Atmos., 120, 4370–4384, doi:10.1002/2014JD022675, 2015. 23102, 23107

UBA: Manual on methodologies and criteria for mapping critical levels/loads and geographical areas where they are exceeded, Federal Environmental Agency (UmweltBundesAmt), the Netherlands, http://www.rivm.nl/en/themasites/icpmm/manual-and-downloads/manual-english/index.html, 2004. 23091

van der Werf, G. R., Randerson, J. T., Giglio, L., Collatz, G. J., Mu, M., Kasibhatla, P. S., Morton, D. C., DeFries, R. S., Jin, Y., and van Leeuwen, T. T.: Global fire emissions and the contribu-

ACPD
15, 23089–23130, 2015

tion of deforestation, savanna, forest, agricultural, and peat fires (1997–2009), Atmos. Chem. Phys., 10, 11707–11735, doi:10.5194/acp-10-11707-2010, 2010. 23095
Vitousek, P. M., Aber, J. D., Howarth, R. W., Likens, G. E., Matson, P. A., Schindler, D. W., Schlesinger, W. H., and Tilman, D. G.: Human alteration of the global nitrogen cycle: sources and consequences, Ecol. Appl., 7, 737–750, doi:10.1890/1051-0761(1997)007[0737:HAOTGN]2.0.CO;2, 1997. 23091
Vries, W. D., Wamelink, G. W. W., Dobben, H. v., Kros, J., Reinds, G. J., Mol-Dijkstra, J. P., Smart, S. M., Evans, C. D., Rowe, E. C., Belyazid, S., Sverdrup, H. U., Hinsberg, A. v., Posch, M., Hettelingh, J.-P., Spranger, T., and Bobbink, R.: Use of dynamic soil–vegetation models to assess impacts of nitrogen deposition on plant species composition: an overview, Ecol. Appl., 20, 60–79, doi:10.1890/08-1019.1, 2010. 23091
Walker, T. W., Jones, D. B. A., Parrington, M., Henze, D. K., Murray, L. T., Bottenheim, J. W., Anlauf, K., Worden, J. R., Bowman, K. W., Shim, C., Singh, K., Kopacz, M., Tarasick, D. W., Davies, J., Gathen, P. v. d., Thompson, A. M., and Carouge, C. C.: Impacts of midlatitude precursor emissions and local photochemistry on ozone abundances in the Arctic, J. Geophys. Res., 117, D01305, doi:10.1029/2011JD016370, 2012. 23097
Wang, Y., Jacob, D. J., and Logan, J. A.: Global simulation of tropospheric O_3-NO_x-hydrocarbon chemistry: 3. Origin of tropospheric ozone and effects of nonmethane hydrocarbons, J. Geophys. Res., 103, 10757–10767, doi:10.1029/98JD00156, 1998. 23095
Wang, Y. X., McElroy, M. B., Jacob, D. J., and Yantosca, R. M.: A nested grid formulation for chemical transport over Asia: Applications to CO, J. Geophys. Res., 109, D22307, doi:10.1029/2004JD005237, 2004. 23095
Wecht, K. J., Jacob, D. J., Wofsy, S. C., Kort, E. A., Worden, J. R., Kulawik, S. S., Henze, D. K., Kopacz, M., and Payne, V. H.: Validation of TES methane with HIPPO aircraft observations: implications for inverse modeling of methane sources, Atmos. Chem. Phys., 12, 1823–1832, doi:10.5194/acp-12-1823-2012, 2012. 23097
Wesely, M.: Parameterization of surface resistances to gaseous dry deposition in regional-scale numerical models, Atmos. Environ., 23, 1293–1304, doi:10.1016/0004-6981(89)90153-4, 1989. 23095
Yienger, J. J. and Levy, H.: Empirical model of global soil-biogenic NOx emissions, J. Geophys. Res., 100, 11447–11464, doi:10.1029/95JD00370, 1995. 23095
Zhang, L., Jacob, D. J., Downey, N. V., Wood, D. A., Blewitt, D., Carouge, C. C., van Donkelaar, A., Jones, D. B. A., Murray, L. T., and Wang, Y.: Improved estimate of the policy-

ACPD
15, 23089–23130, 2015

relevant background ozone in the United States using the GEOS-Chem global model with 1/2° × 2/3° horizontal resolution over North America, Atmos. Environ., 45, 6769–6776, doi:10.1016/j.atmosenv.2011.07.054, 2011. 23095

Zhang, L., Jacob, D. J., Knipping, E. M., Kumar, N., Munger, J. W., Carouge, C. C., van Donkelaar, A., Wang, Y. X., and Chen, D.: Nitrogen deposition to the United States: distribution, sources, and processes, Atmos. Chem. Phys., 12, 4539–4554, doi:10.5194/acp-12-4539-2012, 2012. 23092, 23099, 23101, 23106, 23107

Zhu, L., Henze, D. K., Cady-Pereira, K. E., Shephard, M. W., Luo, M., Pinder, R. W., Bash, J. O., and Jeong, G.-R.: Constraining U.S. ammonia emissions using TES remote sensing observations and the GEOS-Chem adjoint model, J. Geophys. Res. Atmos., 118, 3355–3368, doi:10.1002/jgrd.50166, 2013. 23096, 23097, 23105, 23108

Zhu, L., Henze, D., Bash, J., Jeong, G.-R., Cady-Pereira, K., Shephard, M., Luo, M., Paulot, F., and Capps, S.: Global evaluation of ammonia bi-directional exchange, Atmos. Chem. Phys. Discuss., 15, 4823–4877, doi:10.5194/acpd-15-4823-2015, 2015. 23109

ACPD
15, 23089–23130, 2015

Table 1. NO_x and NH_3 emissions in the contiguous US.

	Sectors	Emissions (Tg N yr^{-1})
NH_3	Total	3.2
	Livestock	2.7
	Fertilizer	0.3
	Natural	0.1
NO_x	Total	4.9
	Surface	2.6
	EGUs*	0.57
	Non-EGU	0.38
	Aircraft	0.13
	Lightning	0.69
	Soil	0.43

* Electric generating units.

ACPD
15, 23089–23130, 2015

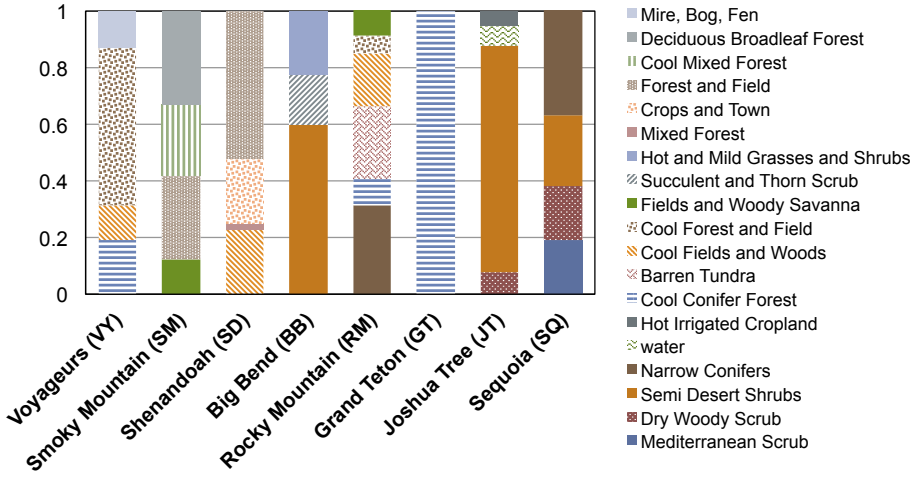

Figure 1. Composition of vegetation types of select Class I areas used in this study based on Olson (1992).

ACPD
15, 23089–23130, 2015

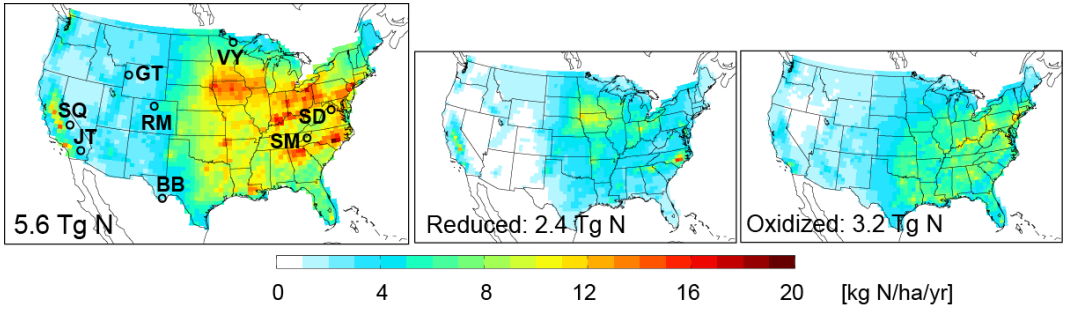

Figure 2. GEOS-Chem modeled Nr deposition in 2010. Select Class I areas for case studies are indicated by initials. Inset number is the annual contiguous US total Nr deposition.

ACPD
15, 23089–23130, 2015

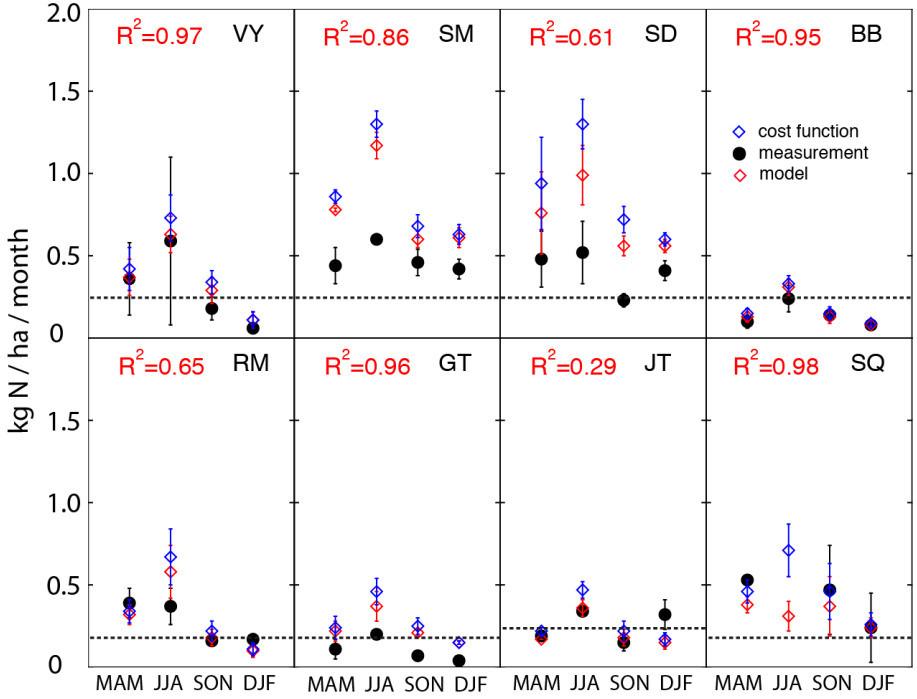

Figure 3. Seasonal variation of Nr deposition in select Class I areas. Model values correspond to only those species that are measured. Cost function values (J_p, open blue diamond) also include dry deposition of NH_3, NO_2, PANs, alkyl nitrate, and N_2O_5. Bars indicate standard deviation of monthly averages in the season. R^2 is squared correlation coefficient for measured and modeled seasonal deposition. Dotted lines are for annual CLs divided by twelve in each site.

ACPD
15, 23089–23130, 2015

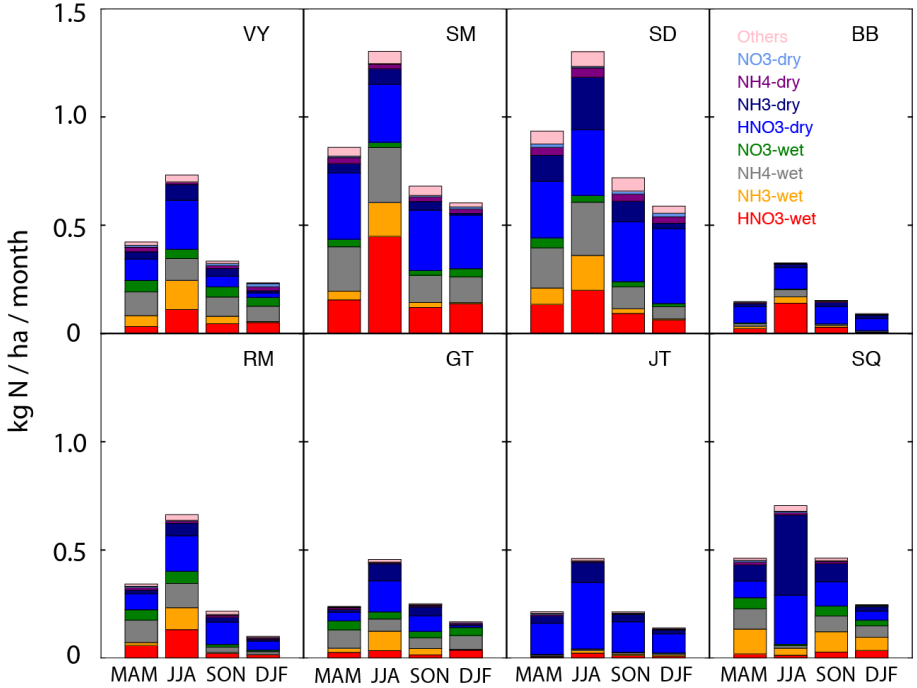

Figure 4. Stacked bar of modeled seasonal Nr deposition showing speciation. Others includes dry deposition of NO_2, PANs, alkyl nitrate, and N_2O_5.

ACPD
15, 23089–23130, 2015

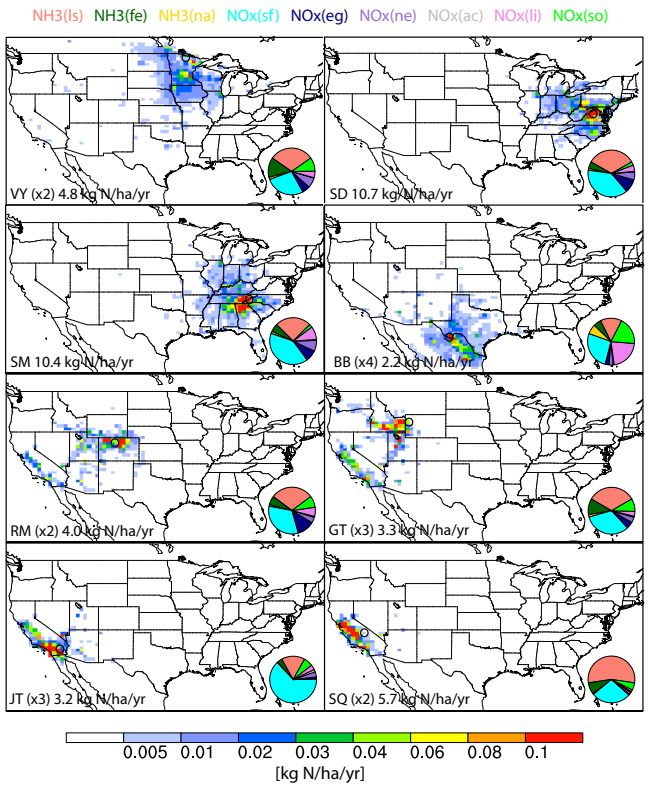

Figure 5. Annual-averaged monthly footprint of Nr deposition in each site and pie chart of fractional contribution from emission sectors. ls: livestock, fe: fertilizer, na: natural, sf: surface inventory, eg: electric generating units, ne: non-eg industrial stacks, ac: aircraft, li: lightning, so: soil. Inset numbers are cost function (J_p), annual Nr deposition in each Class I area. Site locations are shown with open circles. Footprint values are scaled for visibility with numbers in parenthesis.

ACPD
15, 23089–23130, 2015

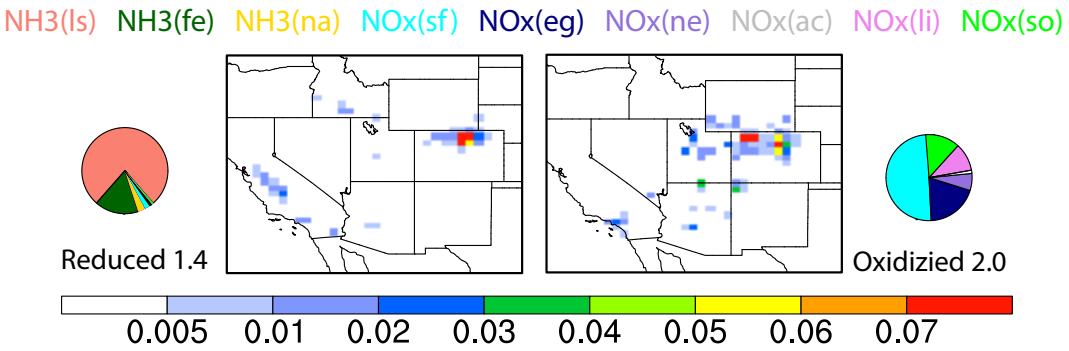

Figure 6. Same as Fig. 5 but for reduced and oxidized Nr deposition in RM. Units for the pie charts and colorbar are kg N/ha/yr. The sum of the oxidized and reduced Nr deposition is smaller than the inset number in Fig. 5 because the number here excludes Nr from "other species".

ACPD
15, 23089–23130, 2015

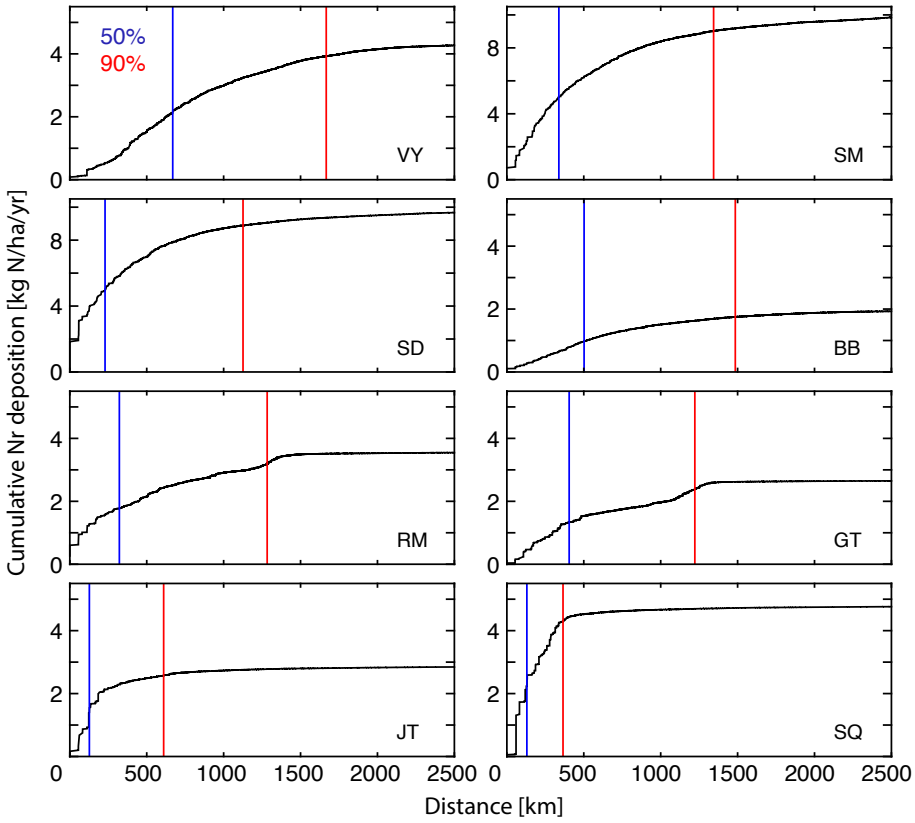

Figure 7. Annual averaged monthly cumulative contribution as a function of distance from the site. Vertical lines are for 50 % (blue) and 90 % (red) of total Nr deposition. Note that the change in scale of the *y* axis for SM and SD.

ACPD
15, 23089–23130, 2015

Sources of nitrogen deposition in Federal Class I areas in the US

H.-M. Lee et al.

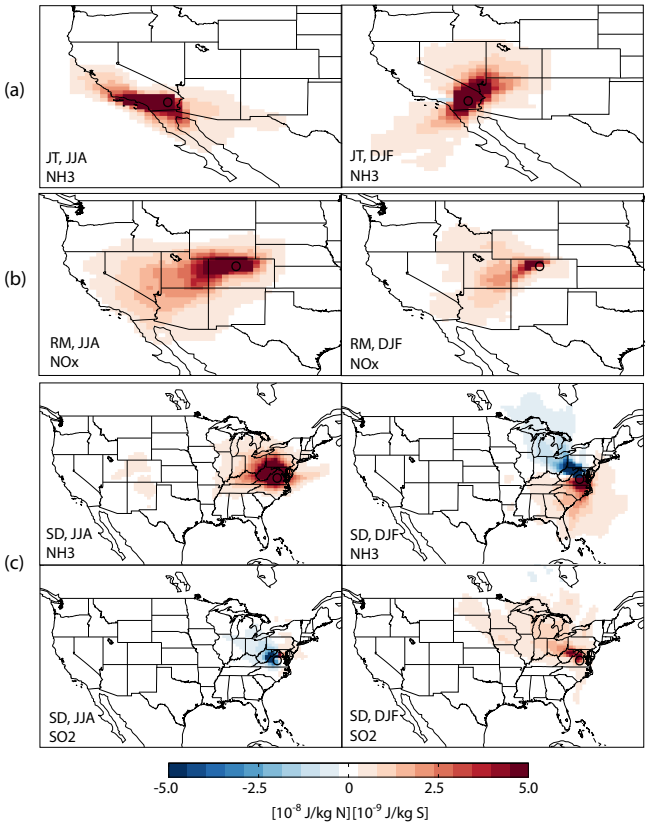

Figure 8. Efficiencies of impacts on Nr deposition showing cost function (J) change per kg N or kg S emission for the tracer and season indicated in the plot. **(a)** Joshua Tree, **(b)** Rocky Mountain, and **(c)** Shenandoah national parks.

ACPD
15, 23089–23130, 2015

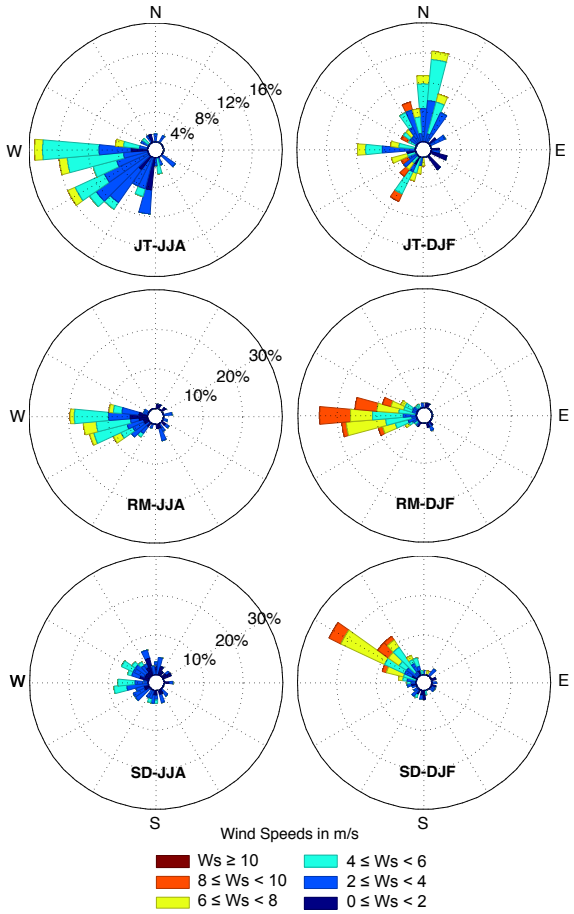

Figure 9. Wind-roses for JT, RM, and SD showing fraction of wind frequencies based on daily surface winds in JJA and DJF.

ACPD
15, 23089–23130, 2015

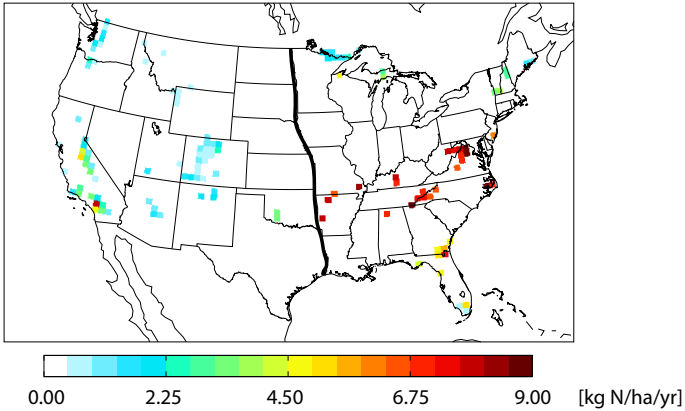

Figure 10. CL exceedance in Class I areas; color indicates magnitude of exceedance. The size of Class I areas are not reflected. Grid cells containing Class I areas are shown as colored regardless of the fraction of Class I areas. Bold line divides Western and Eastern US.

ACPD
15, 23089–23130, 2015

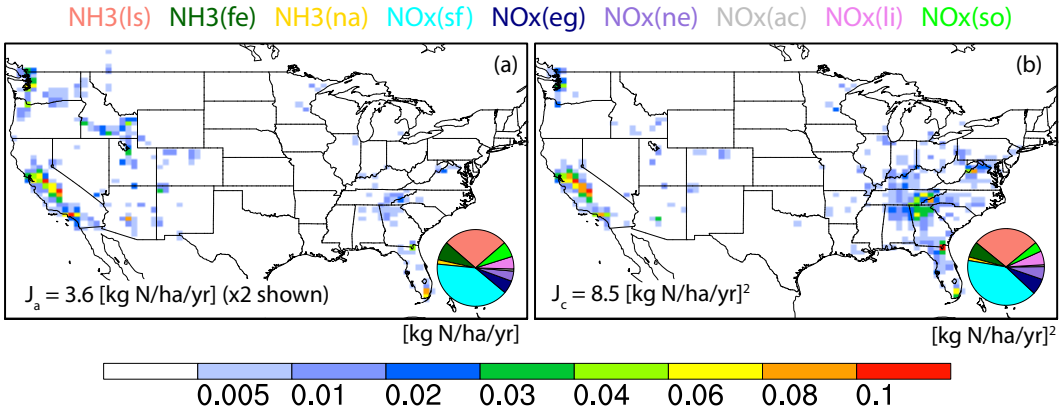

Figure 11. Same figure as Fig. 5 but with different cost functions. **(a)** J_a, **(b)** J_c. Sensitivities of **(a)** are scaled by ×2 to share the colorbar with **(b)**.

ACPD
15, 23089–23130, 2015

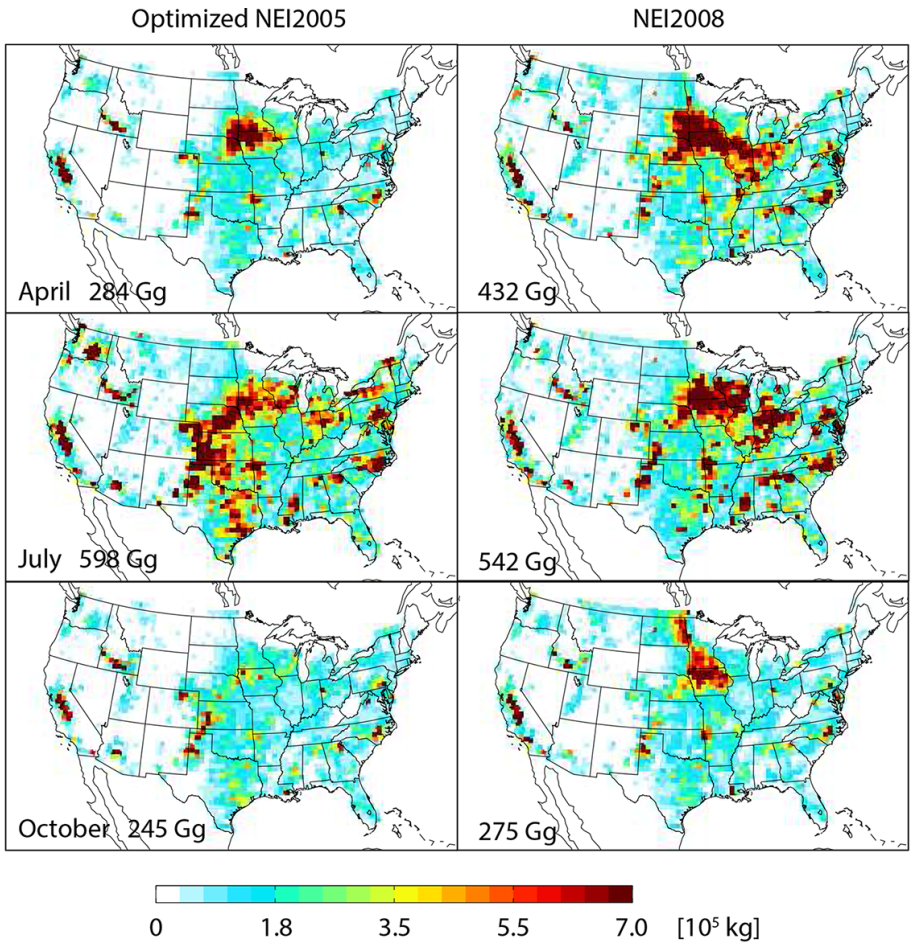

Figure 12. Sum of NH_3 emissions from anthropogenic, natural, biomass burning, and biofuel sources. Inset numbers are contiguous US total NH_3 emissions in each month.

ACPD
15, 23089–23130, 2015

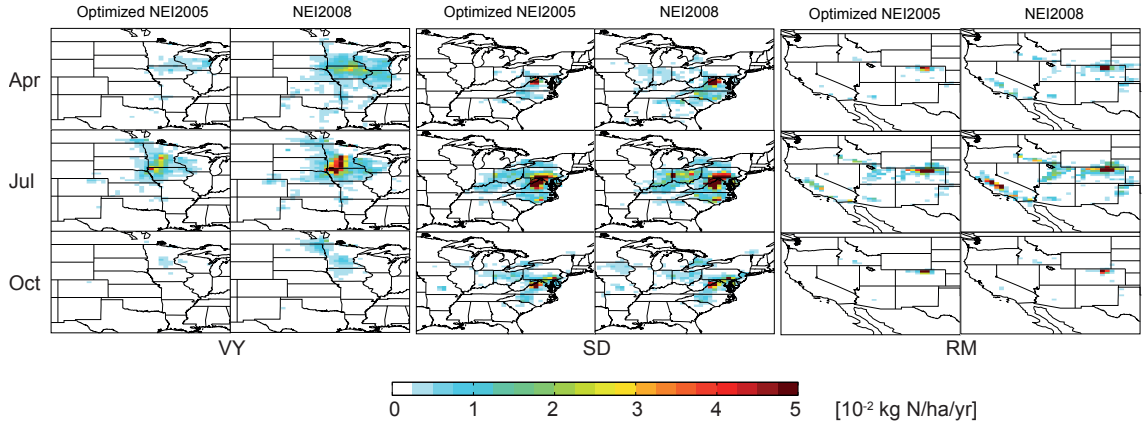

Figure 13. Map of sensitivities of J_p to NH_3 emissions for 3 selected Class I areas (VY, SD, and RM) for two different NH_3 emission inventories (optimized NEI2005 and default NEI2008) in each month.

ACPD
15, 23089–23130, 2015